Journal of Materials Chemistry C

Accepted Manuscript

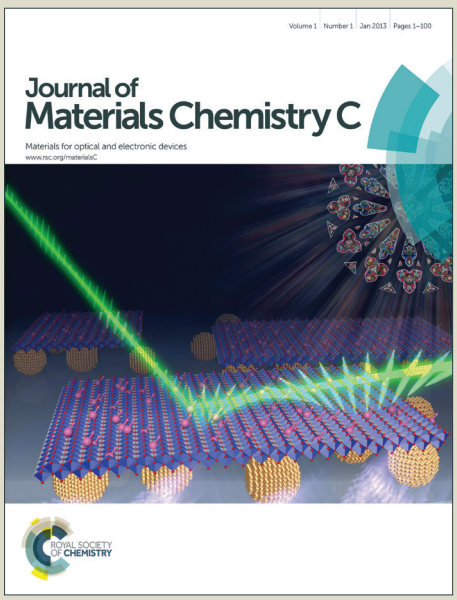

ROYAL SOCIETY OF CHEMISTRY

www.rsc.org/materialsC

Journal of Materials Chemistry C

RSCPublishing

ARTICLE

A comparative Electron Paramagnetic Resonance study of expanded graphites and graphene

Cite this: DOI: 10.1039/xoxxoooooox

Francesco Tampieri[a], Simone Silvestrini[a], Raffaele Riccò[b], Michele Maggini[a], Antonio Barbon[a]*

Received 18th February 2014,
Accepted 00th January 2014

DOI: 10.1039/xoxxoooooox

www.rsc.org/

Graphene, a novel electronic system with unprecedented characteristics, can be obtained with different methods, each producing materials with specific characteristics from the electronic point of view. Among these procedures, methods based on the expansion of graphite allow to obtain graphenic material in rather high quantity. We have then conducted a comparative study of graphenic materials produced by these methods by using Electron Paramagnetic Resonance (EPR) techniques; a single-layer commercial graphene produced with the Hummers method has been used as reference. EPR techniques enable to study some magnetic properties of different types of electrons exhibiting paramagnetic nature. We have analysed the EPR spectra to identify the different types of paramagnetic centres contributing to the spectrum. The analysis of the temperature-dependent EPR spectra and the use of pulse techniques allowed us to separate and characterize the contribution from free conduction electrons from contributions from localized edge states and from molecular-type paramagnetic states.

Introduction

Graphene can be thought as a giant molecule which is available for chemical modification[1, 2] promising for applications ranging from electronics[3-5] to composite materials[4, 6, 7]. Still, there is a wide family of materials between graphene and bulk graphite, from which it was at first isolated[8], with properties depending on different parameters, like the number of stacked layers, their average distance and the dimensions of the ordered clusters[9-12]. At the light of this last observation, the term graphene is nowadays sometimes misused, and in general it represents a class of material characterized by the presence of one to few graphene layers, of limited dimensions, embedded in carbon materials with substitutional groups, or with different ordering (like amorphous phases), often organized in platelets[13], inferring to the material different properties. A key role is played by different types of defects.

Among the materials produced by different methods, in this paper we focus on expanded graphites, since their electronic properties, to the best of our knowledge, have never been studied in detail with the aim of rationalizing the development of the features typical of graphene during the preparation of this technologically important material.

Good quality graphene was first isolated by Geim and Novoselov in 2004[14] using the scotch tape technique, then many other routes were developed. Bottom-up CVD techniques produce nearly defectless materials[15] as mandatory for electronic applications[16]. This synthetic route allows the preparation of extremely pure graphene, with the drawbacks of being quite expensive and convenient for managing only small amounts of material[17-19].

On the other hand, a method that enables to obtain a less expensive material in large quantity is the reduction of graphene oxide (GO)[20], which is usually prepared by the Hummers method[21]. The graphene-like material obtained in this way is very defective with several hydroxyl, carbonyl and carboxyl functional groups along the edges[22]. Moreover, several evidences point towards metal ions residues deriving from the synthesis of GO. In particular, some authors identified the presence Mn(II) ions[23, 24] as a consequence of using potassium permanganate as an oxidant. The same oxidant leaves manganese traces detected in graphene nanoribbons obtained by unzipping carbon nanotubes[16, 25, 26], and an effort is put in finding novel synthetic methods to avoid these impurities[27].

Exfoliation of graphite, which is the method considered here for

[a] Dipartimento di Scienze Chimiche (DiSC), Università degli Studi di Padova, Via Marzolo 1, 35131 Padova (Italy).
E-mail: antonio.barbon@unipd.it. Tel: +39 049 8275151.
[b] CSIRO Division of Material Science and Engineering (CMSE), Private Bag 33, Clayton South MCD, Victoria 3169, Australia.

† Electronic Supplementary Information (ESI) available: XRPD and additional Raman and EPR data. See DOI: 10.1039/b000000x/

the preparation of graphene and graphene-like materials, is another 'top-down' approach[28]. In some way it resembles the original scotch-tape method, seeking to separate carbon monolayers from graphite, but it does so by using a combination of solvents, exfoliating agents and sonication. It has recently gained interest[29] as it enables the production of graphenic materials in relatively high quantity without introducing oxygen defects in the graphene structure. One drawback is that the separation of the graphite sheets is often incomplete. In some cases, to make exfoliation easier, the starting material is functionalized to provide a better interaction with the solvent[6].

Graphite has shown to be a semiconductor with zero band-gap[30, 31]. One of the fundamental works on the magnetic properties of this material is an Electron Paramagnetic Resonance (EPR) work by Wagoner in the late 50's[32] on graphite single crystals, a quasi-ideal system with properties closely conforming to the theory. *Au contraire*, for non-ideal samples of graphitic materials these properties can vary, mostly due to defects.

Edge states, in particular, play an important role in determining the magnetic properties. They are associated to the limited extension of the crystals, being better observed in nanostructured materials[10]. These are non-bonding states localized at the Fermi level[33] and are responsible for the paramagnetic contribution to the magnetization[34].

The same type of defects is expected to play a role on graphene systems as well. Theoretical studies suggest that a crucial role in determining the magnetic properties of graphene is played by localized electron states, or defects[35], which infer anti/ferromagnetic properties to the materials.

The EPR technique is particularly convenient to study in detail the magnetic properties of graphitic and graphenic materials, as it enables to distinguish the contributions from different paramagnetic species. It is rather surprising that the potentialities of this spectroscopy have not been fully exploited yet to study the properties of graphene and related materials. The seminal EPR paper on graphene has appeared in 2009 by L. Ćirić[36]. In that work, graphene sheets obtained by the scotch-tape technique were studied. The authors found a single Lorentzian line (g = 2.0045), with an intensity which varies with the temperature as expected for a zero gap semiconductor ($\chi \propto T$) for T > 70 K due to the thermal promotion of the electron from the valence to the conduction band. More publications on the topic followed, sometimes reporting contradictory results[25, 37]; this is a clear indications that the studied systems are complex, and require the characterization of the nature of the *active sites* responsible for the macroscopic behaviour.

In this paper we show a comparative study of the properties of (*i*) natural graphite, used as a starting material, (*ii*) chemically expanded graphites obtained by different methods based on chemical exfoliation and (*iii*) a commercial sample of reduced graphene oxide consisting of stacks of few graphene layers in the undispersed solid form. We focus in particular on a sophisticated EPR study, to identify paramagnetic defects and conduction electrons.

This study was facilitated both by the availability of materials (gram quantities) and by the presence of many signals with comparable intensity in the EPR spectra, attributable to the different types of paramagnetic species. We are convinced that all the species are present in analogous graphene-related materials, and are responsible for some of the properties of these systems.

Experimentals

Materials

Five different materials were characterized in this study. We started from natural Madagascar graphite, which was used as starting material for the preparation of three processed samples as described below in this section. Finally, we considered a commercial reduced graphene oxide (RGO) for reference.

RGO was received from ACS Materials (MA, USA), labelled 'Single layer Graphene' and used solid without further purification. Natural Madagascar graphite (SM), was kindly provided by Superior Graphite (Chicago, USA). Potassium metal, absolute ethanol, sulphuric acid and nitric acid were acquired from Sigma-Aldrich. All materials were used as received.

Exfoliation of graphite by potassium intercalation and expansion (sample EK). SM (1 g, 83.3 mmol) was loaded in a glass vial with mounted Schlenk-type valve. The vial underwent 3 vacuum-argon cycles, then potassium metal (0.41 g, 10.5 mmol) was loaded under argon flow. After evacuation and three more vacuum-argon cycles, the vial was flame-sealed under vacuum. The tube was set in a tubular oven and heated to 200 °C overnight. The tube was opened in a glove box and the potassium graphite (KC_8) poured in a 100 mL round bottom flask together with 20 mL ethanol. The suspension was stirred for 1 hour, then filtered and washed thoroughly with ethanol to remove potassium ethoxide. The product was finally sonicated in 20 mL ethanol for 8 hours at 150 W, then the solvent was removed under vacuum and the residue dried overnight at 100 °C under vacuum.

Expansion of graphite by acid treatment (sample EH). 100 ml of a 4:1 mixture of sulphuric and nitric acid were loaded in a 250 mL round bottom flask. SM (5 g) was then added and the suspension stirred overnight. The resulting solid was filtered and washed with water to remove excess acid, then irradiated in a microwave apparatus for 40 s at 800 W. The product was dried overnight at 100 °C under vacuum.

Combined expansion-exfoliation (sample EHK). One portion of sample EH underwent further treatment with potassium intercalation and exfoliation in ethanol, following the whole procedure described before for sample EK.

X-ray powder diffraction analysis

X-rays powder diffraction (XRD) transmission patterns were recorded in the diffraction angular range $5° \leq 2\theta \leq 60°$ with a 0.1° resolution, by a Philips X'Pert PRO diffractometer working in the reflection geometry and equipped with a graphite monochromator on

the diffracted beam (CuKα radiation). The full width at half maximum (FWHM) parameters were calculated for most intense peaks by fitting the diffractogram with Lorentzian functions.

Raman measurements

Raman spectra have been recorded with a micro-Raman via a Renishaw spectrometer coupled with an optical microscope. Powder samples were suspended in dichloromethane in an ultrasound bath and drop cast on a standard microscope borosilicate glass plate. After evaporation of the solvent, the spectra were recorded with an excitation wavelength of 622 nm in the 900 to 3200 cm^{-1} range.

EPR measurements

The EPR measurements, cw and pulsed, were obtained with an X-band Bruker ELEXYS spectrometer, equipped with a dielectric resonator and a nitrogen/helium gas-flow cryostat for low temperature measurement. The samples were placed inside 2 or 3 mm ID quartz EPR tubes sealed under vacuum after full evacuation of adsorbed gases. The EPR signals were followed as function of temperature from room temperature (290 K) down to almost the liquid helium temperature (10 K ca.). The field was calibrated using a standard sample with known g-factor (LiTCNQ). The spectra were also corrected taking into account the variation of the quality factor of the resonators with temperature.

The pulsed experiments were performed using the standard pulse sequences: $\pi/2 - \tau - \pi - \tau - echo$ for the electron spin echo (ESE) decay measurement (HD); for the echo detected inversion recovery (IR), instead, the sequence was $\pi - T - \pi/2 - \tau - \pi - \tau - echo$. The resonance field was set at the maximum of the EPR intensity. The Echo-detected EPR (ED-EPR) spectra were obtained by recording the echo intensity as function of the magnetic field. The two pulse electron spin echo envelope modulation (2p-ESEEM) spectra were obtained by Fourier transforming the modulation of the HD, after a proper reconstruction of the signal taking into account the instrumental dead time.

Results

We start with a brief presentation of the structural properties of the SM, EK, EH, EHK and RGO materials, that were investigated by XRD and Raman techniques. While a more in-depth discussion is reported in the Supporting Information material, the comparisons made here are those relevant to understand the intrinsic differences between the various samples that are reflected in the results of EPR experiments presented in the second part of the paragraph.

XRD and Raman results

Reflections in the XRD spectra (reported in the Supporting Information for reference) with Miller index (002) are attributed to different peaks. These are generated by the stacking of the graphenic planes, and were observed near the graphite canonical value of 26.44°. The presence of more than one peak indicates that the samples were a mixture of different graphitic/graphenic structures, with different interlayer distances. According to Bragg law, peaks with lower 2θ values correspond to samples with increased distance between layers. We can separate the peaks in two categories on the base of their width: narrow and broad peaks. Narrow peaks are scattered around the value of 26.44°. These components are present in all but the RGO samples, with slightly different widths and positions. The widths broaden for treated samples, in particular for EK, indicating that the treatment reduces the size of the crystallites. Broad peaks are at lower angular values, and these are present in the RGO as well as in the EK and EHK samples, indicating even smaller crystallites with large interlayer distances. A more detailed analysis of the XRD data is reported in the Supporting Information.

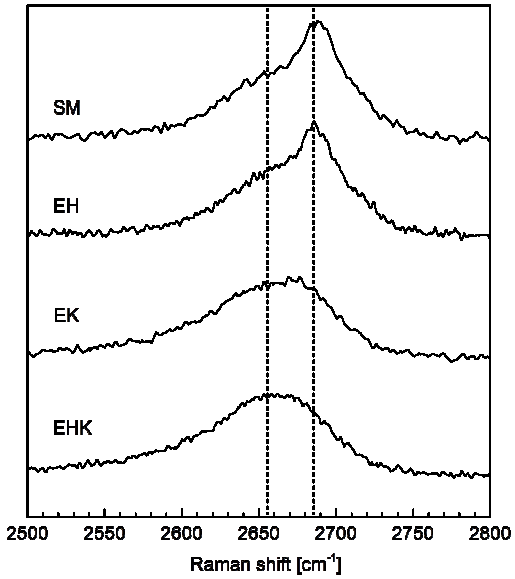

Fig. 1 Raman spectra of 2D band for samples SM, EH, EK and EHK at 622 nm. To guide the eye, the positions of the two major components of EH sample are reported (dotted lines).

In the Raman spectra of the samples, the G bands are observed at 1580 cm^{-1} ca. (the position is shifted to lower values for RGO)[11, 38] while the D bands were recorded at 1320 cm^{-1} ca. The D' bands (1600 cm^{-1} c) and the 2D bands (2700 cm^{-1} ca. see Fig. 1) follow as expected in all cases. The difference in the ratio A(D)/A(G) (see Table 1) between the integrated intensities of the D and the G bands

Table 1 Ratios of the intensities (integrated areas) for bands D and G for the studied samples.

Sample	A(D)/A(G)
RGO	1.78
EH	0.49
EK	1.44
EHK	1.42
SM	0.04

is the first informative aspect emerging from the analysis of the spectra. This ratio is related to the density of the Raman-active defects in the materials. A comparison of the shapes of the 2D bands reported in Fig. 1 of this work can be done with Raman spectra obtained from materials with well-defined structures[11]. The structure of the bands of the two samples, EHK and EK is very similar to that obtained from graphene with very few stacked layers, whereas for EH the shape is more similar to materials with more than 5 stacked layers, and approaches that of graphite.

cw-EPR

The cw-EPR spectra at room temperature for the studied samples are displayed in Fig. 2. All the samples are characterized by the presence of an EPR band with a g factor of ca. 2, typical of organic aromatic systems with low spin-orbit coupling.

Analysis of the spectra have shown that these bands are superpositions of different contribution, each characterized by different parameters. We considered three general situations for the electrons: *a)* non-interacting localized electrons, like in radicals, with small hyperfine (electron-nuclear) interactions, exhibiting Gaussian lineshape, *b)* electrons localized or delocalized in narrow regions, with strong electron-electron interaction, exhibiting Lorentzian lineshape, and *c)* mobile electrons in conductive particles with dimension larger than the microwave penetration depth (skin depth), exhibiting Dysonian lineshape, and normally low intensity.

Due to the heterogeneity of the system and the presence of different types of paramagnetic species, we managed to disentangle different contributions to the observed spectra by fitting the profile *I(B)* as sum of spectra relative to different components with proper normalized lineshape $f(B-B_0)$; typically two components were enough to obtain satisfactory simulations (see Table 2). Assigning a component to a specific species was done *a posteriori*, after careful analysis of the parameters, and of their variation as function of the temperature. We allowed the lineshape profile to be Lorentzian, Gaussian[39, 40] or Dysonian[41, 42] choosing the profile fitting better the data. Moreover we simulated the spectra by taking into account only the Zeeman term of the Hamiltonian[39, 40]. For components with anisotropic **g**-tensor, we calculated the powder spectrum as a superposition of spectra due to spin packets resonating at different fields:

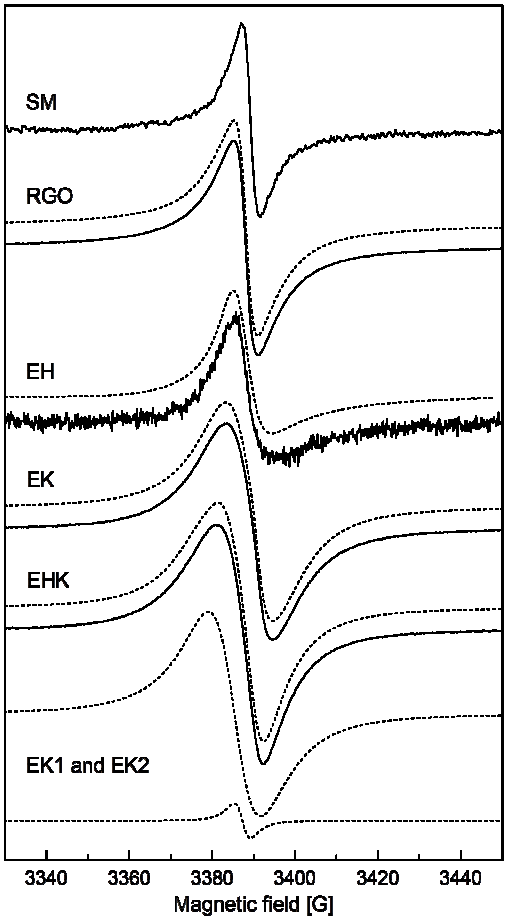

Fig. 2 Normalized cw-EPR spectra of the samples SM, RGO, EH, EK, EHK at room temperature (full lines) together with their simulation (dashed lines). The simulation parameters are reported in Table 2. For sample EK the single components EK1 and EK2 are reported (dotted lines).

Table 2 Relevant simulation parameters of the cw-EPR spectra at room temperature and of the ED-EPR spectra at 80 K. For each contribution i, the linewidth, the perpendicular (subscript label a) and parallel (subscript label b) components of the **g**-tensors are reported (isotropic or parallel, g_{ia}, and perpendicular, g_{ib}); α is the asymmetry parameter for the Dysonian lineshape. The relative abundance of the species (C_i) is indicated.

Sample/ Experiment	T (K)	% C_1	g_{1a}	g_{1b}	Γ_1 [G]	g_{2a}	g_{2b}	Γ_2 [G]	α
RGO / cw-EPR	290	20	2.0031	/	4.4[c]	2.0032	/	13.0[c]	/
EH / cw-EPR	290	82	2.0036	/	17.3[a]	2.0027	/	6.6[b]	1.8
EK / cw-EPR	290	1.6	2.0016	/	3.37[c]	2.0027	/	10.9[c]	/
EHK / cw-EPR	290	28	2.0022	2.0065	5.2[c]	2.0026	2.0093	10.7[c]	/
RGO / ED-EPR	80	100	2.0038	/	1.6	/	/	/	/
EK / ED-EPR	80	13	2.0059	2.0034	2.5	2.0020	2.0097	11.8	/
EHK / ED-EPR	80	9.2	2.0058	2.0018	2.4	2.0040	2.0049	13.3	/

[a] bulk graphite lineshape[32]; [b] general Dysonian lineshape[55]; [c] Lorentzian lineshape

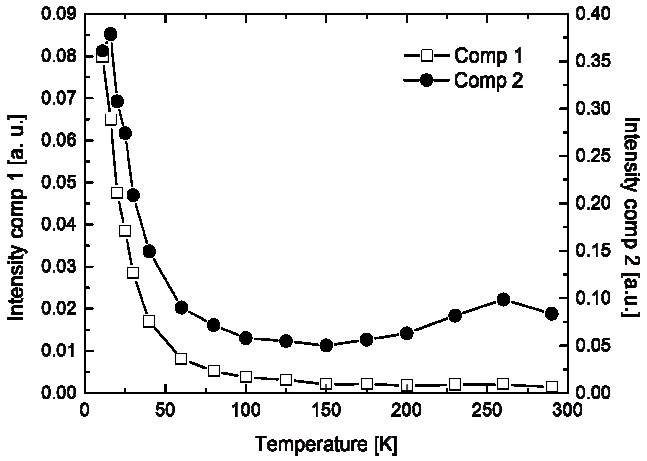

Fig. 3 EPR intensities of the two components of sample EK as function of the temperature (squares: EK-1, circles: EK-2).

$$I(B) \propto \sum_i c_i \int_0^{4\pi} \left[f_i\left(B - B_0(\Omega)\right) \right] d\Omega$$

where B_0 is the resonance fields which depends on the angle Ω between the **g**-tensor axes and the field direction, and the coefficients c_i determine the relative contribution of each spin packet.

For our samples, the parameters of the simulations are reported in Table 2. EH is the only one which displays Dysonian lineshape, typical of conductive samples with particles, or clusters of particles with good electric contact, with dimension larger than the skin depth dependent on the microwave frequency[42] (about 3 μm at X band for bulk graphite[32]). Component EH-1 (82%) was even fitted with the typical lineshape for bulk graphite[32] but in which the anisotropy of the **g**-tensor is lost. As for graphite, an indication of the good conductivity of the sample is given by the wasting of the Q-factor value of the EPR cavity, for which only a small amount of sample could be introduced in it.

The other samples are also conductive, since during sample insertion we observed a considerable deterioration of the Q-factor, but the cw-EPR spectra show Lorentzian lineshapes, indicating that either the dimension of the crystallites is very small compared to the skin depth, or the macroscopic conduction (the mobility of the electrons by jumping between crystallites) of the samples is much lower.

As regards the other samples, only EHK shows anisotropy of the **g**-tensor, with typical values observed in nanographitic samples[10]; in the other cases (EK and commercial RGO) only isotropic signals were observed.

Further information on the nature of the signals is derived from the analysis of the temperature dependence of the cw-EPR spectra, and in particular of the intensity of the different components (Fig. 3). As a matter of fact we can easily distinguish electrons in semiconductors bands from those in localized paramagnetic states, since on lowering the temperature the intensity of the EPR signals of

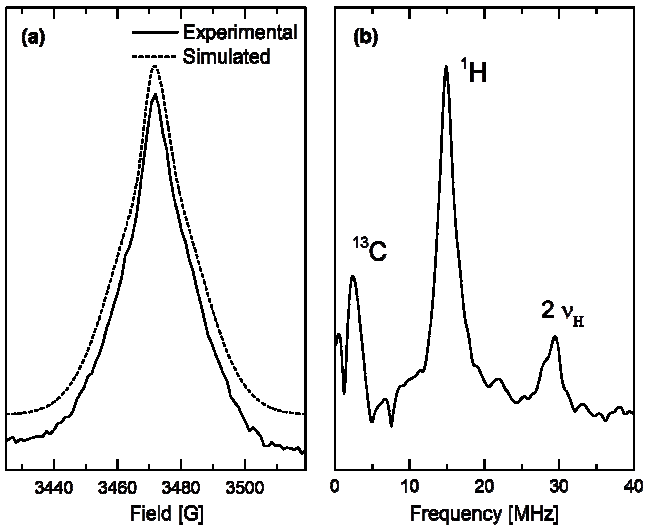

Fig. 4 a) ED-EPR of the sample EHK with τ=200 ns. Two species are present with g-values typical of organic radicals. b) 2p-ESEEM spectrum of sample EHK, it shows the presence of coupled C and H atoms. The spectra are representative also of the samples EK.

the first ones decreases[9], whereas it increases for paramagnetic centres[40].

In general, starting from room temperature, the intensity of the spectra decreases till 100-150 K. For the sample EH below 140 K the signal-to-noise ratio is too weak to be detected. As already pointed out, we associate a decrease of EPR intensity to unpaired electrons in semiconductor bands. A different behaviour is shown by the component EK-1, whose intensity slightly increases, thus showing a small contribution from unpaired electrons in different states. Below 100-150 K the intensity increases for both components with Curie (non interacting electrons) or Curie-Weiss (electron with spin-spin interactions) behaviour[43, 44].

The change in the trend between high and low temperature, is associated with a change of the g-values of the EPR lines. We must conclude that these are due to a complex superposition of signals from different species, whose relative intensity varies in opposite way.

Pulsed EPR

At low temperatures we tried to separate contributions due to species with long spin relaxation times. An analogue attempt at room temperature was unsuccessful.

For samples EK, EHK and RGO we performed pulsed experiments at 80 K; for samples EH and for SM no echo signal could be detected because of the too low signal-to-noise ratio due to the high conductivity of both samples[45]. At first we have recorded ED-EPR spectra. Very similar spectra have been obtained for samples EK, EHK and RGO. In Fig. 4a we report the spectrum for sample EHK. The ED-EPR spectra for samples EK and EHK are composed of two components with Gaussian profile and with axial **g**-tensor, while for sample RGO one Gaussian component with

isotropic **g** was enough to simulate the spectrum. The shape of the spectra was observed to be independent of the delay time between the two pulses. Gaussian lineshapes are normally obtained in the presence of unresolved weak hyperfine interactions. The parameters obtained from the fitting of the spectra are collected in Table 2.

The analysis has then been completed by acquiring the Hahn echo decay for the determination of the phase memory time (T_M), the inversion recovery for the determination of the spin-lattice relaxation time (T_1). We also used hyperfine spectroscopies (ESEEM) to detect eventual couplings with magnetic nuclei for EK, EHK and RGO. The HD and IR traces were fitted using biexponential decay functions:

$$I(t) = A_1 e^{-t/\tau_1} + A_2 e^{-t/\tau_2}$$

where A_i and τ_i are respectively the amplitude and the time constant of the i-th component. The parameters from the fitting of the traces are collected in Table 3.

The HD traces show a modulation due to nuclear interactions with the electron spins. The Fourier transform (FT) of the modulation part resulted in the 2p-ESEEM spectra of the samples (see for example Fig 4b). From these spectra we found the same type of signals for the three samples (EK, EHK and RGO). The spectrum shows two groups of signals, one centred at the resonance frequency of protons (14.9 MHz) and the other at that of ^{13}C nuclei (3.9 MHz). The double frequency peak of protons is visible at 30 MHz.

Discussion

A qualitative view of the EPR results clearly show that each system has proper characteristics, located in the range between the two reference materials: SM and RGO. A more careful overview, given by the use of XRD, Raman and EPR spectroscopies, shows that the samples are rather complex, presenting different structures. In order to rationalize the presented results, it is convenient to discuss them by anticipating such structures and their properties.

Graphite represents the "bulk" boundary for the samples studied in this work. It was first studied by EPR techniques by Wagoner in 1960[32] and with Raman spectroscopy by Tuinstra in 1970[38]. The EPR signal of bulk graphite is due to electrons that are excited to the conduction band, leaving holes behind[32]. The statistics of this system determines a general linear decrease of the magnetization with the lowering of the temperature, reaching a non-zero value at T = 0 K because of a contribution from a Pauli-type magnetization that is temperature-independent[46].

For crystallites with dimension above about 3 μm, the mobile conduction electrons of the particles show a Dysonian EPR-lineshape, due to the skin effect[41, 42]. The **g**-tensor of graphitic materials is highly anisotropic with axial symmetry. The g-components perpendicular to the crystal *c*-axis are almost temperature-independent and their values are near g_e. On the other hand, the parallel component of the tensor is strongly dependent on the temperature with typical values that can reach 2.10 at low temperature for bulk systems[32] and 2.02-2.03 for nano-scale systems[9]. In the latter case, an orientational disorder in the stacking of the graphenic planes can change the g-values. The parallel component of electrons in π-type orbitals is particularly affected, because of the interaction between graphene planes that is responsible for the spin-orbit coupling. For densely packed materials that present a good inter-particle contact, motional averaging can also affect the g-values.

In pure, single layer graphene, obtained by mechanical exfoliation of graphite, EPR signal due to mobile electrons were observed by Ćirić in 2009[36]. Unlike graphite, this signal is symmetric (no skin effect) and it is characterized by an isotropic g-value of 2.003-2.004, closely matching the free electron value g_e.

For graphene, as well as for graphite, it is well known that the limited extension of the π-system generates the so-called edge states, located, in terms of energy, at the contact points between the conduction and the valence bands[47]. These states are not extended throughout the whole π-system, being spatially localized in the proximity of the graphene border. Edge states bear unpaired electrons and are expected to strongly exchange with conduction electrons[48] and with other localized spins[49], thus giving raise to narrow Lorentzian lines.

Unpaired electrons attributable to radicals are expected to be produced in graphenic materials, under strongly reducing conditions. By excluding carbon dangling bonds, observed in diamond-like materials[50] with g = 2.0027, the radicals are likely delocalized systems constituted by carbon, hydrogen and adventitious oxygen. Such radicals have generally isotropic or low-anisotropic **g**-tensors with typical values of 2.003-2.004[51] and can exhibit hyperfine interactions to paramagnetic internal atoms (^1H and ^{13}C) of the order of MHz to kHz, according to the extent of the delocalization.

In the light of the introduction to this section, from an easy

Table 3 Fitting parameters of the HD and IR traces at 80 K.

Sample	Hahn Decay			Inversion Recovery		
	A_1/A_2	τ_1 [μs]	τ_2 [μs]	A_1/A_2	τ_1 [μs]	τ_2 [μs]
RGO	1.88	0.466	3.897	0.60	0.919	7.223
EK	1.09	0.316	1.780	0.67	3.160	30.10
EHK	1.36	0.228	1.180	0.55	1.830	17.20

inspection of the EPR spectra, it is clear that sample EH has rather different behavior with respect to the other exfoliated graphites. The peculiarity of this sample is the high mobility of the electrons through the material, giving rise to a strong decrease in the susceptibility on lowering of the temperature and to a clear Dysonian lineshape due to the larger dimensions of the flakes, compared with the skin depth for graphitic materials. High conduction can be retained through two different mechanisms: delocalization, related to the extent of the wavefunction, and hopping. Because hopping mechanism is likely to be the same in all the materials, we conclude that extension of the wavefunction in large flakes, and likely π-stack interactions, must be responsible of the high mobility of electrons like in graphitic materials. The general reduction of the intensity of the EH-2 component, the dominant contribution to EPR intensity, sustains this hypothesis, backed by XRD and Raman results. The increase in the intensity of component EH-1 shows that some paramagnetic species are also present. Since the characteristics of this sample are closer to SM than to RGO, we conclude that the expansion by treatment with strong acids is not convenient as compared to other methods, for the production of materials with electronic properties resembling those of single layer graphene.

Samples EK and EHK have a more defective sp^2 structure, as suggested by their similar A(D)/A(G) ratio in the Raman spectra, which is larger than that observed for sample EH. This means that they consist of smaller flakes and/or are characterized by a higher concentration of point defects. This becomes particularly evident for RGO. There is a discrepancy between lateral dimensions obtained by XRD and Raman, but that has already been reported[37].

Both Raman and XRD analyses highlight that samples EK and EHK are mixtures of structures, some of which display few-layers stacked graphene sheets, and these are of course the most interesting materials. XRD shows also that exfoliation is not a homogeneous process that leaves some unreacted graphitic structures. We then comment on the information coming out by EPR analysis. The two samples show a wider variety of EPR signals, with some analogies, but also differences, we focus mainly on sample EK.

The EPR intensity of sample EK shows an initial decrease with the lowering of the temperature, passing through a minimum, and quickly rising at the lowest temperatures. This trend can only be interpreted is one assumes the presence of both mobile charge carriers and localized electrons. Regarding the firsts, contributing to EPR at high temperatures, the spectra can be well reproduced using two components with Lorentzian lineshape and isotropic **g**-tensor, close g_e. It is unlikely that this value is obtained by motional averaging, as it should be larger, moreover, the type of lineshape supports the hypotheses of a limited mobility of the electrons, still in the conduction band. We note that one of the two components (EK-2), by far the dominant one, corresponds closely to those found by Ćirić, and to those of RGO sample. In both cases, Lorentzian lineshapes in the range g = 2.003 - 2.004 have been found, with a decrease of the signal by lowering of the temperature. This component can be associated to the most exfoliated fraction of the sample, responsible for the broad, lower-angle contribution of the (002) reflection in the XRD diffractogram.

The other component of EK sample (EK-1) has an unusual g-value, lower than g_e. At the moment we have no clear explanation for this, but we note that such low values are present in other carbon allotropes, like fullerenes and carbon nanotubes, where even lower values can be found[52-54]. These have been associated to the bending of the plane, but to confirm this hypothesis further investigations are required. We can conclude that the signals of sample EK at high temperatures are likely due to electrons in graphenic systems, with well separated layers display only little electronic interactions. This is the major finding of this paper.

At low temperatures, EK resembles RGO better than scotch-tape graphene, the latter having a small Curie-like contribution. The similarity is likewise reflected in the A(D)/A(G) ratio of the Raman spectra. This is not surprising, since it is known from literature that graphene produced by Hummers method is very defective[22]. Indeed, the rise of the intensity due to Curie contributions is much more evident, compared to the material obtained by Ćirić. The disentangling of the signal of sample EK at low temperature enabled to determine the presence of different contributions.

Spin-echo pulse techniques allowed to identify the contributions due to slow relaxing spins, which are estimated to be minority as judged by the echo intensity with respect to cw-EPR intensity. They cannot be edge states, as electrons in these states exhibit strong interactions with other electrons in conduction band, resulting in spin relaxation times $T_1 = T_2$[42]. Moreover, they cannot be the major contribution to the cw-EPR spectra.

Slow relaxing species give an inhomogeneously-broadened spectrum from which it is possible to extract hyperfine interactions with protons and ^{13}C, as determined by the ESEEM spectrum. Moreover, these species are characterized by g-values typical of π-conjugated molecules. We conclude that these signals must be due to sites that have been involved in reactions of the material with hydrides, likely during exposition to the strong reductive environment used for the preparation of the material.

The characteristics of the dominant contribution to the cw-EPR at low temperatures, unlike spin-echo, suggest that they are indeed fast relaxing electrons, and that the linewidth is affected by homogeneous broadening. In all, we propose that the signals of the cw-EPR spectra are then due mostly to electrons in edge states.

Conclusions

We presented a comparative study of a single-layer commercial reduced graphene oxide and graphenic materials produced by different exfoliation processes of graphite. EPR measurement highlighted profound electronic differences between the samples, determined by the different preparation routes. As expected, the

samples presented characteristics intermediate between graphite and graphene.

We were able to separate the contribution to the final EPR spectra of conduction band electrons from electrons related to different types of defects. Both EPR and Raman analyses showed large contributions from defects. Defects in the basal plane affect the electronic properties in different ways, in fact EPR showed that they derive both from edge states and molecular-type species, the latter characterised by the presence of nearby hydrogen, likely introduced in the structure during the production of the material in strong reductive conditions.

Acid exfoliation was the less effective method to obtain good separation of the graphene sheets. On the other hand, intercalation with potassium, followed by reaction with ethanol produced a sample with stronger affinity to RGO in that they display large contribution from conduction electrons and similar g-values and lineshapes. This is an indication that the properties of conduction electrons of EK are closely related to those of graphene, that we associate to a better separation of the graphene layers.

References

1 R. Ruoff, *Nature Nanotechnology,* 2008, **3,** 10-11.
2 K. P. Loh, Q. Bao, P. K. Ang and J. Yang, *Journal of Materials Chemistry,* 2010, **20,** 2277-2289.
3 A. K. Geim and K. S. Novoselov, *Nature Materials,* 2007, **6,** 183-191.
4 A. K. Geim, *Science,* 2009, **324,** 1530-1534.
5 F. Schwierz, *Nature Nanotechnology,* 2010, **5,** 487-496.
6 S. Stankovich, D. A. Dikin, G. H. Dommett, K. M. Kohlhaas, E. J. Zimney, E. A. Stach, R. D. Piner, S. T. Nguyen and R. S. Ruoff, *Nature,* 2006, **442,** 282-286.
7 L. Gong, I. A. Kinloch, R. J. Young, I. Riaz, R. Jalil and K. S. Novoselov, *Adv Mater,* 2010, **22,** 2694-2697.
8 A. C. Neto, F. Guinea, N. Peres, K. Novoselov and A. Geim, *Reviews of Modern Physics,* 2009, **81,** 109.
9 A. Barbon and M. Brustolon, *Applied Magnetic Resonance,* 2012, **42,** 197-210.
10 M. Tommasini, C. Castiglioni, G. Zerbi, A. Barbon and M. Brustolon, *Chemical Physics Letters,* 2011, **516,** 220-224.
11 A. C. Ferrari and D. M. Basko, *Nature Nanotechnology,* 2013, **8,** 235-246.
12 S. Latil and L. Henrard, *Phys. Rev. Lett.,* 2006, **97,** 036803.
13 P. Wick, A. E. Louw-Gaume, M. Kucki, H. F. Krug, K. Kostarelos, B. Fadeel, K. A. Dawson, A. Salvati, E. Vázquez and L. Ballerini, *Angewandte Chemie International Edition,* 2014, .
14 K. Novoselov, A. K. Geim, S. Morozov, D. Jiang, Y. Zhang, S. Dubonos, I. Grigorieva and A. Firsov, *Science,* 2004, **306,** 666-669.
15 X. Tong, C. Xie, L. Si, J. Che and Y. Xiao, *Mater. Chem. Phys.,* 2013, **143,** 85-92.
16 D. V. Kosynkin, A. L. Higginbotham, A. Sinitskii, J. R. Lomeda, A. Dimiev, B. K. Price and J. M. Tour, *Nature,* 2009, **458,** 872-876.
17 S. Bhaviripudi, X. Jia, M. S. Dresselhaus and J. Kong, *Nano Letters,* 2010, **10,** 4128-4133.
18 H. Cao, Q. Yu, R. Colby, D. Pandey, C. Park, J. Lian, D. Zemlyanov, I. Childres, V. Drachev and E. A. Stach, *J. Appl. Phys.,* 2010, **107,** 044310-044310-7.
19 P. R. Somani, S. P. Somani and M. Umeno, *Chemical Physics Letters,* 2006, **430,** 56-59.
20 S. Stankovich, D. A. Dikin, R. D. Piner, K. A. Kohlhaas, A. Kleinhammes, Y. Jia, Y. Wu, S. T. Nguyen and R. S. Ruoff, *Carbon,* 2007, **45,** 1558-1565.
21 W. S. Hummers Jr and R. E. Offeman, *J. Am. Chem. Soc.,* 1958, **80,** 1339-1339.
22 V. Singh, D. Joung, L. Zhai, S. Das, S. I. Khondaker and S. Seal, *Progress in Materials Science,* 2011, **56,** 1178-1271.
23 A. M. Panich, A. I. Shames, A. E. Aleksenskii and A. Dideikin, *Solid State Commun.,* 2012, **152,** 466-468.
24 B. S. Paratala, B. D. Jacobson, S. Kanakia, L. D. Francis and B. Sitharaman, *PLoS One,* 2012, **7,** e38185.
25 S. Rao, A. Stesmans, D. Kosynkin, A. Higginbotham and J. Tour, *New Journal of Physics,* 2011, **13,** 113004.
26 A. Hirsch, *Angewandte Chemie International Edition,* 2009, **48,** 6594-6596.
27 C. V. Pham, M. Krueger, M. Eck, S. Weber and E. Erdem, *Appl. Phys. Lett.,* 2014, **104,** 132102.
28 M. J. Allen, V. C. Tung and R. B. Kaner, *Chem. Rev.,* 2009, **110,** 132-145.
29 Y. Hernandez, V. Nicolosi, M. Lotya, F. M. Blighe, Z. Sun, S. De, I. McGovern, B. Holland, M. Byrne and Y. K. Gun'Ko, *Nature Nanotechnology,* 2008, **3,** 563-568.
30 C. Coulson, *Nature,* 1947, **159,** 265-266.
31 P. Wallace, *Physical Review,* 1947, **71,** 622.
32 G. Wagoner, *Physical Review,* 1960, **118,** 647.
33 T. Makarova and F. Palacio, *Carbon Based Magnetism: An Overview of the Magnetism of Metal Free Carbon-Based Compounds and Materials,* Elsevier Science, 2006.
34 V. Y. Osipov, A. Shames, T. Enoki, K. Takai, M. Endo, T. Hayashi, Y. Kaburagi and A. Y. Vul, *Diamond and Related Materials,* 2009, **18,** 220-223.
35 R. Nair, M. Sepioni, I. Tsai, O. Lehtinen, J. Keinonen, A. Krasheninnikov, T. Thomson and A. G. I. Grigorieva, *Nature Physics,* 2012, **8,** 199-202.
36 L. Ćirić, A. Sienkiewicz, B. Nafradi, M. Mionić, A. Magrez and L. Forro, *Physica Status Solidi (B),* 2009, **246,** 2558-2561.
37 H. R. Matte, K. Subrahmanyam and C. Rao, *The Journal of Physical Chemistry C,* 2009, **113,** 9982-9985.
38 F. Tuinstra and J. L. Koenig, *J. Chem. Phys.,* 1970, **53,** 1126.
39 P. W. Atkins and J. De Paula, *Atkins' Physical Chemistry,* Oxford University Press Oxford, 2006.
40 N. M. Atherton and N. Atherton, *Electron Spin Resonance: Theory and Applications,* Ellis Horwood Chichester, 1973.
41 G. Feher and A. Kip, *Physical Review,* 1955, **98,** 337.
42 F. J. Dyson, *Physical Review,* 1955, **98,** 349.
43 A. F. Orchard, *Magnetochemistry,* Oxford University Press, 2003.
44 M. Ruitenbeek, A. Barbon, E. Van Faassen and J. Geus, *Catalysis Letters,* 1998, **54,** 101-104.
45 M. Brustolon, *Electron Paramagnetic Resonance: A Practitioner's Toolkit,* John Wiley & Sons, 2009.
46 N. W. Ashcroft and N. D. Mermin, *Electron spin resonance: theory and applcations,* Ellis Horwood Chirchester, 1973.
47 M. Fujita, K. Wakabayashi, K. Nakada and K. Kusakabe, *Journal of the Physical Society of Japan,* 1996, **65,** 1920-1923.
48 V. J. Joly, K. Takahara, K. Takai, K. Sugihara, T. Enoki, M. Koshino and H. Tanaka, *Physical Review B,* 2010, **81,** 115408.
49 M. Braun, P. Struck and G. Burkard, *Physical Review B,* 2011, **84,** 115445.
50 D. Keeble and B. Ramakrishnan, *Appl. Phys. Lett.,* 1996, **69,** 3836-3838.
51 B. H. Bielski and J. M. Gebicki, *Atlas of Electron Spin Resonance Spectra,* Academic Press, 1967.

52 P. Allemand, G. Srdanov, A. Koch, K. Khemani, F. Wudl, Y. Rubin, F. Diederich, M. Alvarez, S. Anz and R. Whetten, *J. Am. Chem. Soc.,* 1991, **113,** 2780-2781.
53 M. M. Khaled, R. T. Carlin, P. C. Trulove, G. R. Eaton and S. S. Eaton, *J. Am. Chem. Soc.,* 1994, **116,** 3465-3474.
54 A. Thess, R. Lee, P. Nikolaev, H. Dai, P. Petit, J. Robert, C. Xu, Y. H. Lee, S. G. Kim and A. G. Rinzler, *Science-AAAS-Weekly Paper Edition,* 1996, **273,** 483-487.
55 J. P. Joshi and S. Bhat, *Journal of Magnetic Resonance,* 2004, **168,** 284-287.

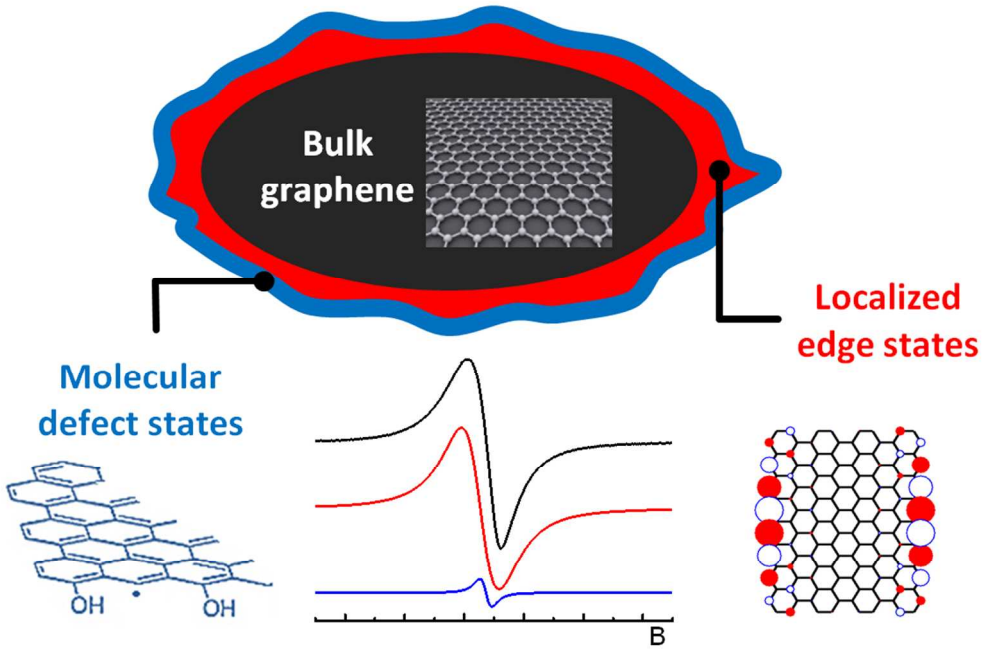

EPR techniques enable the disentangling of signals belonging to different types of structures.